Generation and characterization of ionic and neutral [HS–P–OH]+/· and S=P(OH)2+/· in the Gas Phase by Tandem Mass Spectrometry and Computational Chemistry

ARTICLE *in* JOURNAL OF THE AMERICAN SOCIETY FOR MASS SPECTROMETRY · APRIL 2002

Impact Factor: 2.95 · DOI: 10.1016/S1044-0305(01)00360-9 · Source: PubMed

6 AUTHORS, INCLUDING:

Ragampeta Srinivas
Indian Institute of Chemical Technology
171 PUBLICATIONS **1,390** CITATIONS
SEE PROFILE

Frantisek Turecek
University of Washington Seattle
237 PUBLICATIONS **9,680** CITATIONS
SEE PROFILE

Generation and Characterization of Ionic and Neutral [HS-P-OH]$^{+/\cdot}$ and S=P(OH)$_2^{+/\cdot}$ in the Gas Phase by Tandem Mass Spectrometry and Computational Chemistry

R. Srikanth, P. Nagi Reddy, K. Bhanuprakash, and R. Srinivas
Indian Institute of Chemical Technology, Hyderabad, India

Xiaohong Chen and Frantisek Tureček
Department of Chemistry, University of Washington, Seattle, Washington, USA

Dissociative electron ionization of diethyl dithiophosphate (**I**) and O,O′-diethyl methylphosphonothioate (**II**) generates moderately abundant *m/z* 81 ions of composition [P, O, S, H_2]$^+$. From tandem mass spectrometry experiments and theoretical calculations at the B3LYP/6-31G(d,p), G2, and G2 (MP2) levels it is concluded that the majority of the ions have the structure of HS-P-OH$^+$ (**1a**$^+$) and it is separated by high-energy barriers from its isomers P(= S)OH_2^+ (**1b**$^+$), P(= O)SH_2^+ (**1c**$^+$), HP(= S)OH$^+$ (**1d**$^+$), and HP(= O)SH$^+$ (**1e**$^+$). Low-energy (metastable) ions **1a**$^+$ dissociate via losses of H_2O and H_2S to yield *m/z* 63 (PS^+) and *m/z* 47 (PO^+) product ions, respectively. These reactions involve isomerization of **1a**$^+$ into the stable isomers **1b**$^+$ and **1c**$^+$. Neutralization-reionization experiments confirm the theoretical prediction that radical **1a**$^\cdot$ is a stable species in the gas-phase. Variable-time NR experiments indicated that only a small fraction of metastable **1a**$^\cdot$ radicals dissociate in the 0.4–4.6 μs time window, while most dissociations occurred on a shorter time scale. RRKM calculations were performed to investigate unimolecular dissociation kinetics of **1a**$^\cdot$ which were found to be in agreement with the fragmentation observed in the NR spectrum. The 70-eV electron ionization of (**I**) and diethyl chlorothiophosphate (**III**) yields *m/z* 97 ions, predominantly of the structure S = P$(OH)_2^+$ (**2a**$^+$). This conclusion follows from tandem mass spectrometry experiments and theoretical calculations. The calculations predict that (**2a**$^+$) is separated by high-energy barriers from its isomers O = P(SH)OH$^+$ (**2b**$^+$), S = P(= O)OH_2^+ (**2c**$^+$), and O = P(= O)SH_2^+ (**2d**$^+$). Neutralization-reionization experiments confirmed that **2a**$^\cdot$ radical is a kinetically stable species on the time scale of up to 5 μs, which is in agreement with ab initio calculations. However, owing to a mismatch of Franck-Condon factors a large fraction of **2a**$^\cdot$ dissociates by loss of SH$^\cdot$ yielding O = P − OH. (J Am Soc Mass Spectrom 2005, 16, 1353–1366) © 2005 American Society for Mass Spectrometry

Over the past 15 years, a great deal of attention has been focused on the chemistry of phosphorus oxoacids, some of which belong to the family of low-coordination phosphorus compounds. Phosphorus oxoacids are believed to play an important role in the chemistry and biochemistry of phosphorus and have been extensively studied by experiment and theory [1–5]. Low-coordination dithiophosphanes are also known to be reactive intermediates and some of them have been isolated as stable ligands in complexes [6, 7]. Unfortunately, direct evidence for the existence of these species as stable monomeric entities is scarce because of facile intermolecular reactions. The neutralization-reionization mass spectrometry (NRMS) technique [8–14] has been established as a powerful tool for investigating the stabilities and structures of highly reactive and elusive transient species in the rarefied gas-phase, and it has been successfully used to generate and characterize some of the low coordinated phosphorus species. Keck, Terlouw and their coworkers have provided NRMS experimental evidence for the gas-phase existence of (methylthio) thioxophosphane (CH_3S-P-S) [15], phosphenethiol (H_2P-SH) [16], phosphenedithiol HP$(SH)_2$ [17], thioxophosphane HPS and its tautomer HSP [18] and phosphorotrithious acid P$(SH)_3$ [19] molecules. Gu and Tureček [20] have reported an NRMS study on several oxygenated phosphorus radicals, e.g., PO, CH_3OPH, CH_3OPOH, CH_3OPOCH_3, and $(CH_3O)_2$PO. Vivekananda, Srinivas, and coworkers reported on the generation and charac-

Published online June 23, 2005

Address reprint requests to Dr. R. Srinivas, National Center for Mass Spectrometry, Indian Institute of Chemical Technology, Hyderabad 500007, India. E-mail: srini@ins.iictnet.com

This article is registered as IICT Communication No. 050224.

1044-0305/05/$30.00
doi:10.1016/j.jasms.2005.03.021

Received February 18, 2005
Revised March 15, 2005
Accepted March 19, 2005

terization of low coordinated phosphorus species, viz., $CH_3O-P=O$, $CH_3S-P=O$ and NH_3PO by using a combination of tandem mass spectrometric techniques [21, 22]. Tureček et al. have also demonstrated the importance of Franck-Condon effects in the dissociations and isomerizations of gas-phase phosphorus oxoacids and radicals, mainly $P(OH)_3$ and $P(OH)_4$. and their corresponding isomeric species [23]. This NRMS study revealed that vertical neutralization of stable $P(OH)_4^+$ produced vibrationally excited unstable $P(OH)_4^{\cdot}$, whereas the tricoordinated $P(OH)_3^{+\cdot/o}$ and its isomer $HPO(OH)_2^{+\cdot/o}$ formed stable molecules on the microsecond time scale of NRMS experiments. A number of theoretical calculations were also reported on these tri- and tetra-coordinated hydroxy and thiohydroxy phosphoranyl species [24–31]. We recently reported on the characterization of ionic and neutral $P(OH)_2^{+/\cdot}$ and the corresponding isomeric species by NRMS and computational chemistry [32]. In continuation of our studies, we report here on the generation and characterization of both ionic and neutral $[HS\text{-}POH]^{+/\cdot}$ and $[S=P(OH)_2]^{+/\cdot}$.

Experimental

Most mass spectrometric experiments reported here were carried out using a VG Micromass Autospec M mass spectrometer of E_1BE_2 geometry [21] (E denotes an electric sector and B the magnetic sector). The instrument has two collision chambers (Cls-2 and Cls-3) and an intermediate deflector electrode, all in the third field free region (between E_1B and E_2).

Diethyl dithiophosphate (**I**), O,O′-diethyl methylphosphonothioate (**II**), and diethyl chlorothiophosphate (**III**) were commercially available (Aldrich, Steinheim, Germany) and used without further purification. All the compounds were introduced into the ion source through the liquid inlet system under the following conditions: source temperature, 200 °C; electron energy, 70 eV; trap current 200 μA; acceleration potential, 7 kV. Accurate mass measurements of the ions at *m/z* 81 from **I** and **II** and *m/z* 97 from **I** and **III** were obtained at a resolution of $m/\Delta m = 5000$ (10% valley definition), using the data system. The collision induced dissociation (CID) mass spectra were recorded by mass selecting the beam of interest ions using E_1B (MS-1), with 7 keV translational energy and allowing collisions with oxygen in the collision cell Cls-3, the resulting ions were analyzed by scanning E_2 (MS-2). CID mass spectra were also recorded in the FFR-1 using the linked scan technique (B/E = constant). The MS/MS/MS experiments were performed by allowing the precursor ions to dissociate in the FFR-1 (preceding E_1) and transmitting the fragment ions formed there into the FFR-3, where a CID spectrum was obtained using Cls-3. The NR experiments were conducted by mass selecting the beam ions of studied with E_1B (MS-1) and neutralizing them in Cls-2 with xenon. The remaining ions were deflected away from the beam of neutrals by means of a deflector electrode (+5 kV). The neutral beam was reionized in Cls-3 with O_2 target gas and the resulting ions were recorded by scanning E_2. The spectra shown are accumulations of 25–50 scans. Kinetic energy release measurements were performed from peak widths at half-height ($T_{0.5}$) and corrected for the precursor beam width.

Another set of NR mass spectra were measured on the tandem quadrupole acceleration-deceleration mass spectrometer described previously [33]. Samples were introduced into the electron-ionization ion source from a glass inlet system at room temperature. The ionization conditions were as follows: emission current: 1 mA, electron energy: 70 eV, ion source temperature: 200 °C. Ions were accelerated to 7200 eV and neutralized by collisions with dimethyl disulfide that was admitted to the first collision cell at pressures allowing 70% transmittance of the ion beam. Residual ions were reflected by applying +250 V on a lens, and neutral intermediates were allowed to drift 60 cm to the reionization cell where a fraction was reionized by collisions with O_2 at 70% beam transmittance. The ions formed were decelerated to 75–80 eV, energy filtered, and analyzed by a quadrupole mass analyzer that was floated at 70–75 V and operated at unit mass resolution. Thirty to fifty scans were typically accumulated and averaged in the NR mass spectra. Variable-time NR mass were recorded by gating the voltages on the elements of the ion conduit placed between the neutralization and reionization cells [34, 35]. The neutral lifetimes were 0.44, 1.3, 2.2, and 4.6 μs for precursor ions at *m/z* 81, and 0.48, 1.4, 2.4, and 5.0 μs for precursor ions at *m/z* 97.

Computational Methodologies

Standard ab initio and density functional methods included in the Gaussian 03 [36] suites of programs were used to calculate the geometries and relative stabilities of ions and their corresponding neutral isomers. In the density functional methods, Becke's hybrid functional, B3LYP with the 6-31G(d,p) basis set was used initially for geometry optimizations [37], while in the ab initio methods G2 [38] and G2(MP2) [39] schemes were used. Stationary points were characterized as either minima (all real frequencies) or transition states (one imaginary frequency) by calculation of the frequencies using an analytical gradient procedure. The minima connected by given transition structures were confirmed by intrinsic reaction coordinate (IRC) calculations. The calculated frequencies were also used to determine zero-point vibrational energies, which were used as a zero-point correction for the electronic energies. Spin unrestricted calculations were used for all open shell systems and the spin contamination was not found to be high (0.75–0.76) for doublets.

Selected ion and neutral species were also optimized with B3LYP and the larger 6-311 ++ G(2d,p) basis set. Single point energies for this set were calculated using

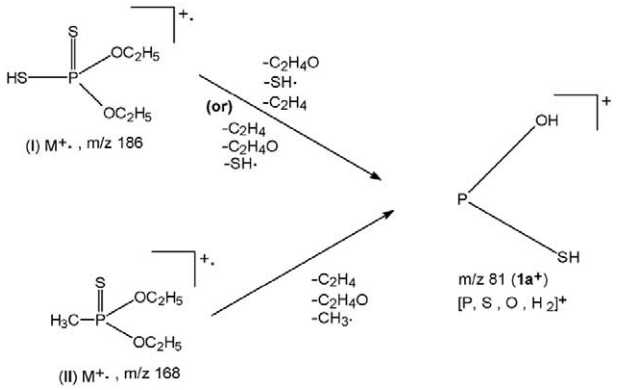

Scheme 1

Moller-Plesset theory [40] truncated at second-order with valence-only electron excitation and with spin annihilation for open shell-systems [41], PMP2, using the 6-311 ++ G(3df,2p) basis set. Coupled-cluster theory [42] with single, double, and perturbational triple excitations, CCSD(T) [43], and the 6-311 ++ G(d,p) basis set was used to calculate another set of single-point energies. The PMP2/6-311 ++ G(3df,2p) and CCSD(T)/6-311 ++ G(d,p) single-point energies were combined as in the G2(MP2) scheme to provide effective CCSD(T)/6-311++G(3df,2p) energies. These were corrected for zero-point vibrational energies and, together with the B3LYP/6-311 ++ G(2d,p) moments of inertia and harmonic frequencies, used for Rice-Ramsperger-Kassel-Marcus (RRKM) calculations of unimolecular rate constants [44]. The RRKM calculations used Hase's program [45] that was recompiled and run under Windows XP [46]. Rotational states were treated adiabatically and the microscopic rate constants, k(E,J,K), were Boltzmann averaged for the distribution of rotational states at 473 K, which was the ion source temperature. The canonical rate constants, k(E), were used for the calculations of branching ratios.

Results and Discussion

Preparation and Dissociation of [P,S,O,H$_2$]$^+$ Ions

The 70-eV electron-ionization mass spectra of diethyl dithiophosphate (**I**), and O,O′-diethyl methylphosphonothioate (**II**) afford a moderately abundant peak at *m/z* 81 (20 and 10% of the base peak, respectively) corresponding to [P,S,O,H$_2$]$^+$ ions. The elemental composition of this ion has been confirmed by high-resolution measurements, and isobaric impurities were not detected. The formation of these ions from the diethyl dithiophosphate (I$^{+\cdot}$) can be envisaged to proceed by two different pathways, (1) 186$^{+\cdot}$ (**I**$^{+\cdot}$) → 142$^{+\cdot}$ → 109$^+$ → 81$^+$, i.e., loss of C_2H_4O followed by successive losses of SH$^\cdot$ radical and ethylene molecule, (2) 186$^{+\cdot}$ (**I**$^{+\cdot}$) → 158$^{+\cdot}$ → 114$^{+\cdot}$ → 81$^+$, i.e., loss of ethylene molecule followed by C_2H_4O and a SH$^\cdot$ radical. For **II**$^{+\cdot}$, the *m/z* 81 ions are generated by the route: 168$^{+\cdot}$ (**II**$^{+\cdot}$) → 140$^{+\cdot}$ → 96$^{+\cdot}$ → 81$^+$, i.e., loss of ethylene followed by C_2H_4O and a $CH_3\cdot$ radical (Scheme 1). Evidence for these pathways follows from metastable ion (MI) spectra of the molecular ions and the intermediate ions.

The *m/z* 81 ions were characterized by MI and CID spectra; the latter were recorded as B/E and MIKE scans (Figure 1a and b). Besides obvious differences in mass resolution in these scans, the B/E and MIKE CID spectra sampled precursor ions of different life times. The metastable-ion spectrum shows PS$^+$ (*m/z* 63) and PO$^+$ (*m/z* 47) ions as dominant fragments corresponding to losses of H_2O and H_2S, respectively. These MI peaks showed simple gaussian profiles which were

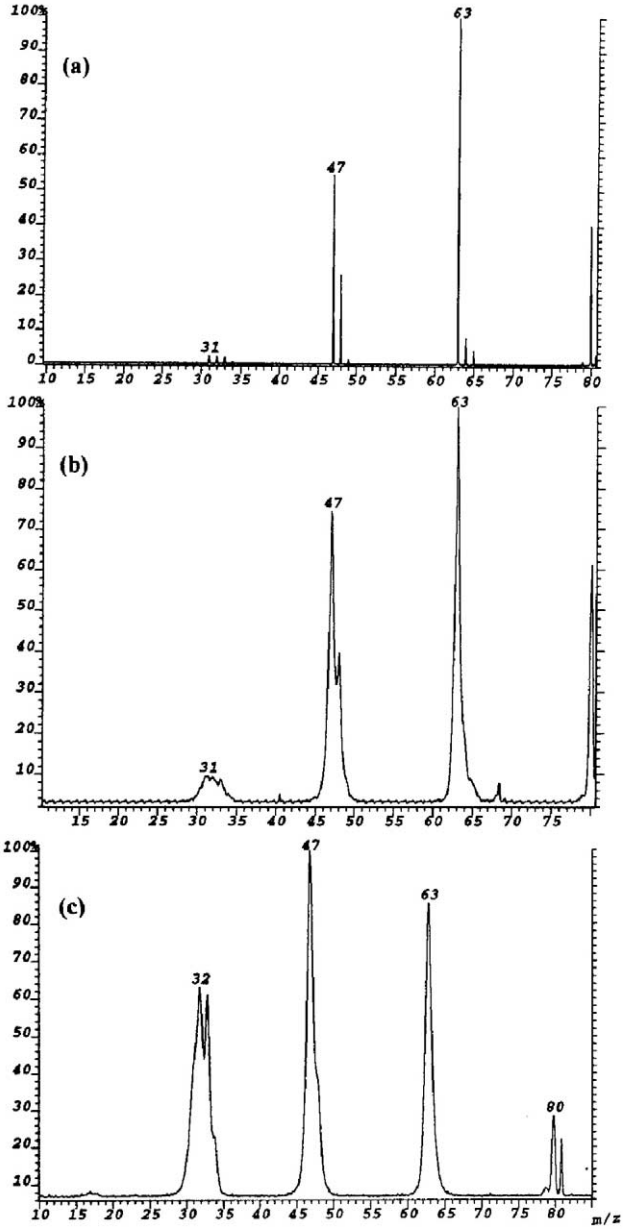

Figure 1. (**a**) B/E-CID spectrum (O_2, 70% transmission), (**b**) MIKES-CID spectrum (O_2, 70% transmission), and (**c**) NR spectrum (Xe, 70% T/O_2, 70% transmission) of *m/z* 81 ions from diethyl dithiophosphate (**I**).

characterized by the values of kinetic energy release at half-maximum, $T_{0.5}$ = 0.144 eV (144.6 meV) and 0.102 eV (102.6 meV), respectively. These results indicate that *m/z* 81 ions probably do not correspond to a mixture of isomers, and that losses of H_2O and H_2S involve tight transition states.

The CID spectra (B/E and MIKE) display the base peak at *m/z* 63 (PS^+) due to loss of H_2O and other abundant fragment ions are $[P,O,S,H]^{+\cdot}$ at *m/z* 80 (loss of $H^\cdot$), $[POH]^+$ at *m/z* 48 (loss of $SH^\cdot$) and $[PO]^{+\cdot}$ at *m/z* 47 (loss of H_2S). Losses of H_2O and H_2S are the characteristic peaks in the CID spectra of phosphorus ions, containing −OH and −SH, respectively. For example, $P(OH)_2^+$ ion dissociates by loss of H_2O, and $P(SH)_3^+$ ion dissociates by loss of H_2S [32, 19]. Weaker-intensity peaks are observed at *m/z* 65 $[P,S,H_2]^+$, *m/z* 64 $[P,S,H]^+$, *m/z* 49 $[P,O,H_2]^+$, and a cluster of peaks at *m/z* 31–33 attributable to P^+, $S^{+\cdot}$, and SH^+. With all these structure indicative peaks, the spectra are most compatible with the HS—P—OH^+ (**1a**$^+$) bond connectivity for the *m/z* 81 ions. The CID spectra of the *m/z* 81 ions from O,O′-diethyl methylphosphonothioate (**II**) are identical with those from diethyl dithiophosphate (**I**).

Loss of C_2H_4 is the only dissociation of the metastable *m/z* 109 ion ($C_2H_5OPSH^+$) from $\mathbf{I}^{+\cdot}$ and the internal energy content of the resulting *m/z* 81 ions is expected to be lower than that of the source generated ions. Therefore, the metastably generated *m/z* 81 ions from the *m/z* 109 precursor ion may well represent isomerically pure ions **1a**$^+$. This MS/MS/MS spectrum (not shown), although of low sensitivity, is found to be closely similar to that in Figure **1b**, suggesting that the source generated *m/z* 81 ions are largely **1a**$^+$.

Table 1. Relative energies of $[P, S, O, H_2]^+$ ions

	Relative energy[a]		
Species	G2	G2 (MP2)	B3LYP[bc]
PSH(OH)$^+$ (**1a**$^+$) (C_S)	0	0	0
P(=S)OH_2^+ (**1b**$^+$) (C_1)	25	23	15
P(=O)SH_2^+ (**1c**$^+$) (C_1)	69	69	56
HP(=S)OH$^+$ (**1d**$^+$) (C_S)	41	41	58
HP(=O)SH$^+$ (**1e**$^+$) (C_S)	105	106	118
TS **1a**$^+$ → **1b**$^+$ (C_1)	134	133	124
TS **1a**$^+$ → **1c**$^+$ (C_1)	184	182	179
TS **1a**$^+$ → **1d**$^+$ (C_1)	206	207	218
TS **1a**$^+$ → **1e**$^+$ (C_1)	—	—	310
TS **1d**$^+$ → **1b**$^+$ (C_1)	270	268	266
TS **1c**$^+$ → **1e**$^+$ (C_1)	302	301	308
TS **1d**$^+$ → **1e**$^+$ (C_1)	241	237	264
$PS^+ + H_2O$ *m/z* 63	105	102	132
$PO^+ + H_2S$ *m/z* 47	187	184	186
$POH^{+\cdot} + SH$ *m/z* 48	380	385	335
$SPOH^{+\cdot} + H^\cdot$ *m/z* 80	380	382	366
$PSH^{+\cdot} + OH^\cdot$ *m/z* 64	484	476	434

[a]In units of kJ mol^{-1} at 0 K.
[b]Calculations with the 6-31G(d,p) basis set.
[c]ZPE corrected.

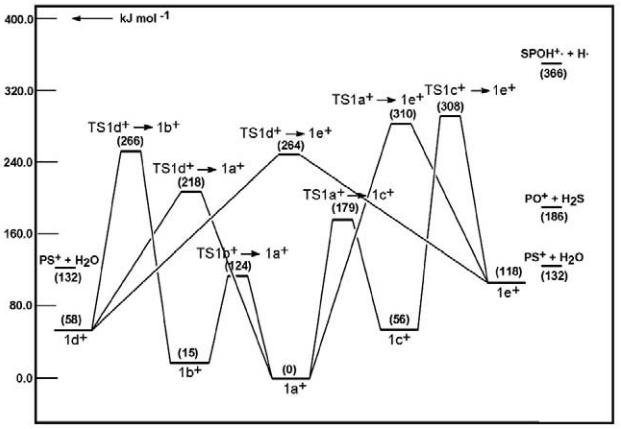

Scheme 2. Potential energy diagram from B3LYP/6-31G(d,p) calculations for the rearrangement and dissociation reactions of ions **1a**$^+$ to **1e**$^+$.

Ion Structures and Energetics

To interpret the experimental data from ion dissociations, we investigated by calculations the potential energy surface for dissociations and isomerizations of all possible isomers **1a**$^+$–**1e**$^+$ (Table 1). The results from B3LYP/6-31G(d,p) calculations are summarized diagrammatically in Scheme **2**; the optimized ion structures and transition-state geometries are shown in Fig-

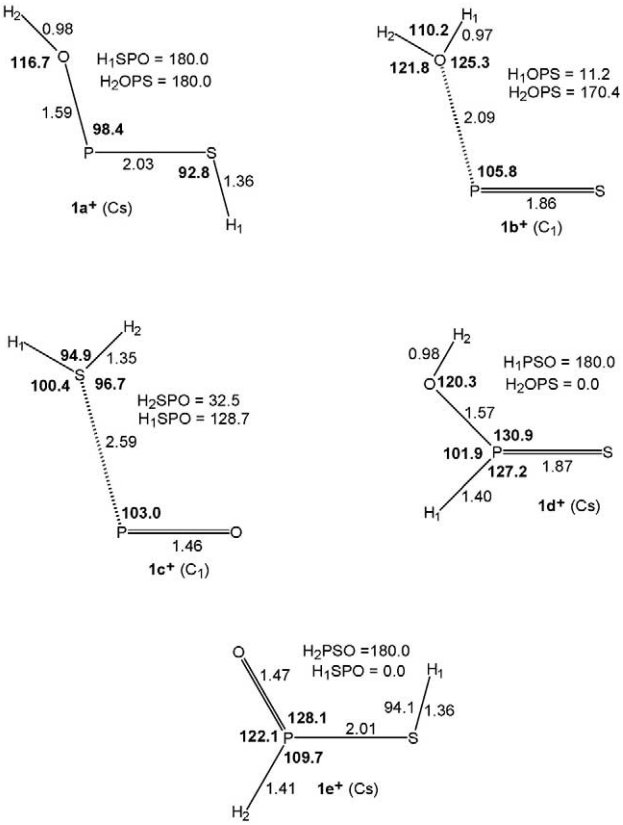

Figure 2. Selected optimized geometries of ionic $[P, S, O, H_2]^+$ isomers **1a**$^+$–**1e**$^+$ from B3LYP/6-31G(d,p) calculations.

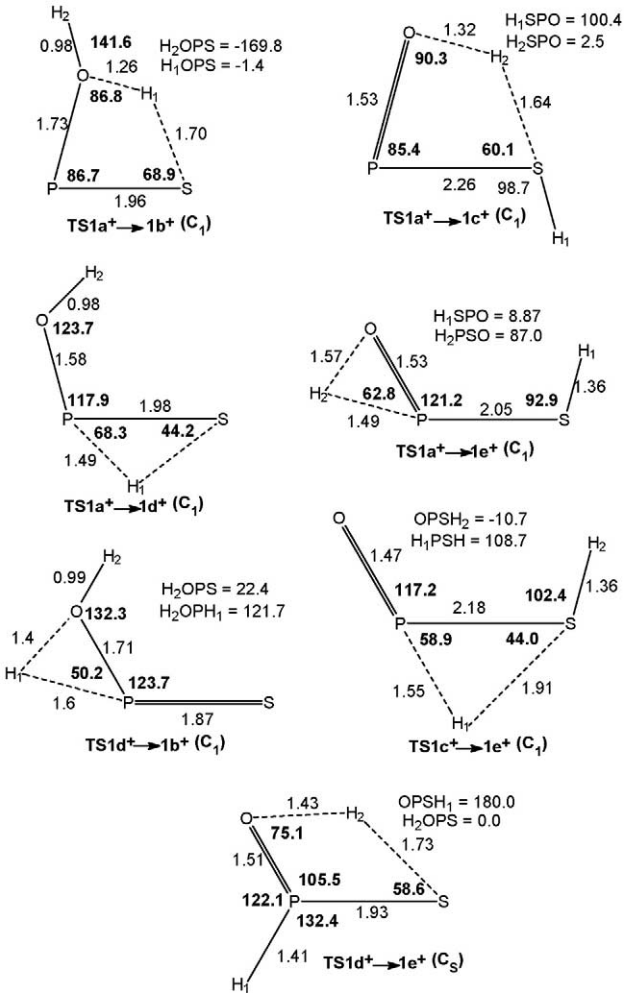

Figure 3. Selected transition-state geometries of ionic [P, S, O, H_2]$^+$ isomers **1a**$^+$–**1e**$^+$ from B3LYP/6-31G(d,p) calculations.

ures 2 and 3. Ion **1a**$^+$ is the most stable structure of the five studied. It has a C_S symmetry with an anti-anti arrangement of the O—H and S—H bonds that corresponds to the lowest-energy orientation of the corresponding bond dipoles. **1b**$^+$ is second most stable structure, 15 kJ mol^{-1} less stable than **1a**$^+$. The P—OH_2 bond in **1b**$^+$ is about 30% longer than a standard P—O bond, indicating a preferred dissociation to PS^+ and H_2O which requires 132 kJ mol^{-1}. Ions **1a**$^+$ and **1b**$^+$ are separated by an energy barrier (109 kJ mol^{-1} above **1b**$^+$), which is below the lowest dissociation threshold for the formation of PS^+ + H_2O (Scheme 2). Similarily, **1c**$^+$, 56 kJ mol^{-1} less stable than **1a**$^+$, has a longer P—SH_2 bond (28% longer than a standard P—S bond) and can preferably dissociate into PO^+ and H_2S which requires 186 kJ mol^{-1}. Ions **1a**$^+$ and **1c**$^+$ are separated by an energy barrier (123 kJ mol^{-1} above **1c**$^+$), which is below the dissociation energy for the formation of PO^+ + H_2S. Thus the calculated energies imply that **1a**$^+$ having sufficient internal energy can isomerize to **1b**$^+$ and **1c**$^+$ before dissociating and display similar MI and CID spectra. Ions **1d**$^+$ and **1e**$^+$ are less stable than **1a**$^+$ by 58 and 118 kJ mol^{-1}, respectively, and are separated from the latter by energy barriers (160 kJ mol^{-1} above **1d**$^+$ and 192 kJ mol^{-1} above **1e**$^+$, respectively), which are substantially above the lowest dissociation threshold. Hence, the possibility of interconversion of **1a**$^+$ → **1d**$^+$ and **1a**$^+$ → **1e**$^+$ ions is unlikely. Nevertheless, a minor fraction of **1d**$^+$ and **1e**$^+$ ions may be formed which can dissociate into $SPOH^+$ + H$^\cdot$. This is a highly endothermic process, requiring 366 kJ mol^{-1} which is in keeping with the low abundance of *m/z* 80 compared with that of *m/z* 63 in the CID spectrum. Thus, based on all these results, it can be proposed that the CID spectra of *m/z* 81 ions represent a mixture of **1a**$^+$/**1b**$^+$/**1c**$^+$ ions. However, for energetic and entropic reasons most of the ions are expected to have the connectivity **1a**$^+$. We have also investigated triplet states which were found to be much less stable than the singlets, and therefore, only the latter are considered. For example, ^{3}**1a**$^+$ is found to be less stable than ^{1}**1a**$^+$ by 208 kJ mol^{-1}.

Preparation and Dissociation of [P,S,O,H_2]$^\cdot$ Radicals

The neutralization (Xe, 70%)-reionization (O_2, 70%) mass spectrum of *m/z* 81 ions shows a moderately abundant recovery signal corresponding to the survivor ions of reionized [P,S,O,H_2] radicals (Figure 1c). The spectrum shows all the fragment ions that are seen in the CID spectrum of Figure 1b, except that the relative abundances of *m/z* 63 is decreased and those of *m/z* 47, 34, 33, and 32 are increased in the NR spectrum. Weakly abundance peaks at *m/z* 16–18 are also present in the spectrum. This can be attributed to a combination of low kinetic energy causing scattering losses and lower reionization efficiency and high ionization energy of water molecules. The presence of a moderately abundant recovery signal indicates that vertical neutralization of **1a**$^+$ ions yield neutral species that are stable on the NR experimental time-scale of microseconds and have retained the **1a**$^\cdot$ connectivity. The difference in the abundances of the fragment ions may be due to the contribution from the dissociation of excited [P,S,O,H_2] radicals, as will be dis-

Table 2. Calculated adiabatic energies (IE_a) and vertical one-electron transition energies (in eV) of ions and neutrals of [P, S, O, H_2]$^{+/\cdot}$ isomers at B3LYP/6-31G(d,p) level

Transitions	IE_a	RE_v	IE_v
1a$^+$ → **1a**$^\cdot$	7.39	7.09	
1a$^\cdot$ → **1a**$^+$			8.45
1b$^+$ → **1b**$^\cdot$	7.15	6.77	
1b$^\cdot$ → **1b**$^+$			7.56
1c$^+$ → **1c**$^\cdot$	7.17	6.91	
1c$^\cdot$ → **1c**$^+$			7.40
1d$^+$ → **1d**$^\cdot$	7.97	6.96	
1d$^\cdot$ → **1d**$^+$			8.98
1e$^+$ → **1e**$^\cdot$	8.23	7.06	
1e$^\cdot$ → **1e**$^+$			9.29

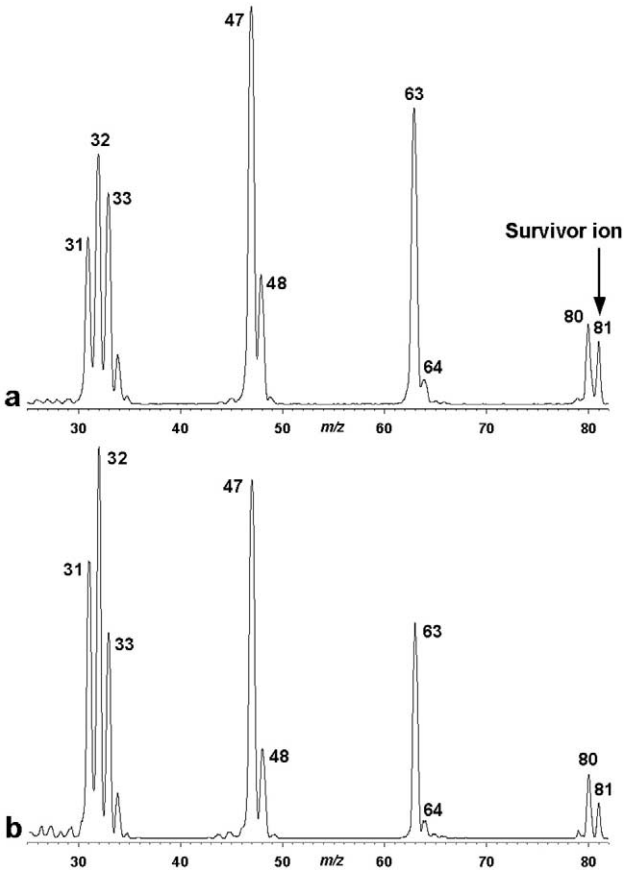

Figure 4. Neutralization (70% transmittance)/reionization O_2 (70% transmittance) mass spectra of $\mathbf{1a}^+$ at (**a**) 4.6 μs and (**b**) 0.44 μs neutral dissociation times. Low-intensity peaks at *m/z* 26–29 are due to low-level isobaric hydrocarbon contaminants.

cussed later in the paper. The calculated recombination energies of ion structures $\mathbf{1a}^+$–$\mathbf{1e}^+$ (Table 2), predict that the electron-transfer from Xe (IE = 12.13 eV) is 4.5–5.0 eV endothermic, which may also cause excitation in the radicals formed.

To further investigate this effect, we obtained NR mass spectra of $\mathbf{1a}^+$ with dimethyl disulfide as the neutralization gas whose IE_v = 8.96 eV is closer to the recombination energy of the phosphorus radicals. Figure 4a shows a dissociation pattern which is very similar to that from neutralization with Xe. The NR mass spectrum in Figure 4a displays a survivor ion at *m/z* 81 attesting to a fraction of stable radicals. Major dissociation products are due to loss of H (*m/z* 80), OH (*m/z* 64), H_2O (*m/z* 63), HS (*m/z* 48 and 33), and H_2S (*m/z* 47 and 34). Variable-time spectra, as represented by the spectrum obtained at 0.44 μs (Figure 4b), show increased relative abundance of low-mass fragments at *m/z* 31–34 and a slightly smaller [*m/z* 81]/[*m/z* 80] ratio, compared with the same ions in the NR mass spectrum obtained at 4.6 μs (Figure 4a). These results indicate that there is only a small fraction of metastable [P,O,S,H_2] radicals that would dissociate in the 0.4–4.6 μs time interval, while most dissociations occurred on a shorter time scale. The increased overall fragmentation at shorter drift times for neutrals is probably due to longer time scales for ion dissociations.

Table 3. Relative energies of [P, S, O, H_2]$^{\cdot}$ radicals

Species	Relative energy[a]			
	G2	G2 (MP2)	B3LYP[bc]	CCSD(T)[cde]
PSH(OH)$^{\cdot}$ (**1a**$^{\cdot}$) (C_1)	0	0	0	0
P(=S)$OH_2^{\cdot}$ (**1b**$^{\cdot}$) (C_1)	43	41	43	42
P(=O)SH_2 of (**1c**$^{\cdot}$) (C_1)	71	72	78	74
HP(=S)OH$^{\cdot}$ (**1d**$^{\cdot}$) (C_S)	1	3	2	−4
HP(=O)SH$^{\cdot}$ (**1e**$^{\cdot}$) (C_S)	29	27	39	29
TS **1a**$^{\cdot}$ → **1b**$^{\cdot}$ (C_1)	123	118	107	120
TS **1a**$^{\cdot}$ → **1c**[b] (C_1)	143	143	145	143
TS **1a**$^{\cdot}$ → **1d**$^{\cdot}$ (C_1)	89	87	93	89
TS **1a**$^{\cdot}$ → **1e**$^{\cdot}$ (C_1)	187	187	181	188
TS **1d**$^{\cdot}$ → **1b**$^{\cdot}$ (C_1)	193	191	172	
TS **1c**$^{\cdot}$ → **1e**$^{\cdot}$ (C_1)	166	167	137	142
TS **1d**$^{\cdot}$ → **1e**$^{\cdot}$ (C_1)	140	136	152	
TS **1a**$^{\cdot}$ → S---H				152
TS **1d**$^{\cdot}$ → P---H				146
PS$^{\cdot}$ (*m/z* 63) + H_2O	59	56	66	39
PO$^{\cdot}$ (*m/z* 47) + H_2S	81	81	92	84
SPOH (*m/z* 80) + H$^{\cdot}$	141	137	164	140
POH (*m/z* 48) + SH$^{\cdot}$	330	336	321	
PSH (*m/z* 64) + OH$^{\cdot}$	382	384	378	

[a]In units of kJ mol^{-1} at 0 K.
[b]Calculations with the 6-31G(d,p) basis set.
[c]ZPE corrected.
[d]Calculations with the 6-311 ++ G(3df,2p) basis set.
[e]Effective energies from linear extrapolation: *E*[CCSD(T)/6-311++G(3df,2p)] = *E*[CCSD(T)/6-311 ++ G(d,p)] + *E*[PMP2/6-311 ++ G(3df,2p)] − *E*[PMP2/6-311 ++ G(d,p)].

Radical Structures and Energetics

These experimental results are consistent with the theoretical calculations (Table 3 and Scheme **3**), which show **1a**$^{\cdot}$ and **1d**$^{\cdot}$ as the two most thermodynamically stable radical isomers (Figures 5 and 6). The relative 0 K enthalpies for **1a**$^{\cdot}$ and **1d**$^{\cdot}$ depend on the level of theory;

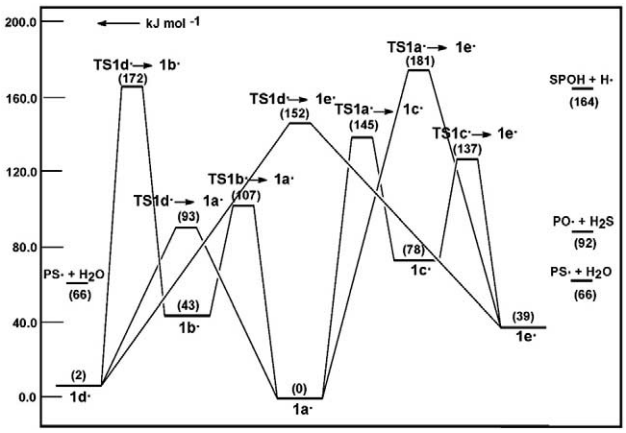

Scheme 3. Potential energy diagram from B3LYP/6-31G(d,p) calculations for the rearrangement and dissociation reactions of neutrals **1a**$^{\cdot}$ to **1e**$^{\cdot}$.

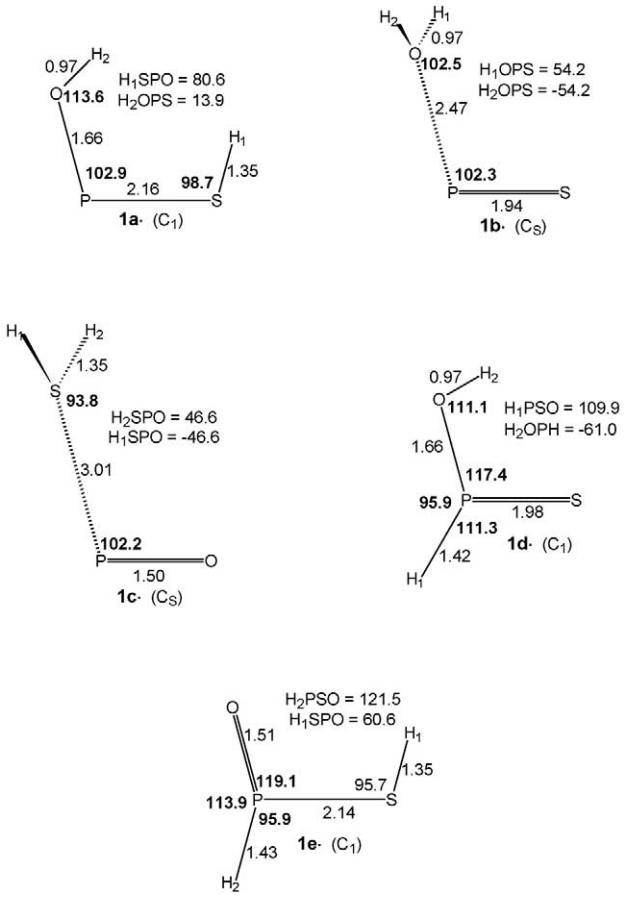

Figure 5. Selected optimized geometries of neutral [P, S, O, H_2]$^{\cdot}$ isomers **1a**$^{\cdot}$–**1e**$^{\cdot}$ from B3LYP/6-31G(d,p) calculations.

at the highest CCSD(T) level, **1d**$^{\cdot}$ is more stable by 3.9 kJ mol^{-1}. However, **1a**$^{\cdot}$ is favored entropically, so that the free-energy difference, $\Delta G°_T$(**1a**$^{\cdot}$ → **1d**$^{\cdot}$), increases from −1.9 kJ mol^{-1} at 300 K to 0.7 kJ mol^{-1} at 500 K where **1a**$^{\cdot}$ becomes more stable. Radicals **1b**$^{\cdot}$, **1c**$^{\cdot}$, and **1e**$^{\cdot}$ are 42, 74, and 29 kJ mol^{-1}, respectively, less stable than **1a**$^{\cdot}$ at 0 K (Table 3). In addition, **1a**$^{\cdot}$ is separated from the other isomers by substantial energy barriers for interconversion (Scheme 3). The lowest barrier for isomerization to **1d**$^{\cdot}$ is calculated by CCSD(T) at 89 kJ mol^{-1}, while the barriers for isomerizations to **1b**$^{\cdot}$ and **1c**$^{\cdot}$ are even higher at 120 and 143 kJ mol^{-1}, respectively. The latter two transition-state energies are above the dissociation thresholds for **1b**$^{\cdot}$ → PS$^{\cdot}$ + H_2O (ΔH_0 = 39 kJ mol^{-1} relative to **1a**$^{\cdot}$) and **1c**$^{\cdot}$ → PO$^{\cdot}$ + H_2S (ΔH_0 = 84 kJ mol^{-1} relative to **1a**$^{\cdot}$). This indicates that **1b**$^{\cdot}$ and **1c**$^{\cdot}$ formed by unimolecular isomerization of **1a**$^{\cdot}$ would have sufficient energy to dissociate and could not isomerize back to the more stable isomer **1a**$^{\cdot}$. The isomerization barrier for **1a**$^{\cdot}$ → **1d**$^{\cdot}$ is below the transition states for the other isomerizations, as well as below the lowest transition-state energy for direct dissociation of **1a**$^{\cdot}$ to HO-P = S and H$^{\cdot}$ (E_{TS} = 152 kJ mol^{-1}) (Table 3). Thus, a fraction of non-dissociating **1a**$^{\cdot}$ in the energy interval 89–120 kJ mol^{-1} can undergo reversible isomerization to **1d**$^{\cdot}$. However, kinetic and equilibrium ΔG calculations show **1a**$^{\cdot}$ to be more stable than **1d**$^{\cdot}$ at these excitation energies, and so the former is predicted to be the dominating isomer even in the fraction that can isomerize. The energy analysis suggests that a predominant fraction of non-dissociating [P,O,S,H_2] radicals exist as structure **1a**$^{\cdot}$ which is represented by the survivor ion in the NR spectrum.

Further support for the stability of the transient neutral comes from an examination of the Franck-Condon effects on vertical electron capture by the corresponding cations. For **1a**$^{+}$, the calculated vertical ionization energy of the neutral (IE_V) is found to be 102 kJ mol^{-1} (Table 2) higher than the adiabatic process, and vertical neutralization (RE_V) of thermalized HS—P—OH^{+} ions differ by only 29 kJ mol^{-1} from the adiabatic process. The minimum excess Frank-Condon energy of HS—P—OH$^{\cdot}$ is only 29 kJ mol^{-1}, which is insufficient to induce any dissociation or isomerization as the threshold energy of dissociation or isomerization lies at higher energies (Table 2). Thus the observed recovery signal in the NR spectrum should correspond to the **1a**$^{\cdot}$ survivor ions. In contrast, vertical neutralization of **1b**$^{+}$ leads to the formation of excited radicals of **1b**$^{\cdot}$ having an internal energy of 37 kJ mol^{-1} which is sufficient to induce fragmentation in to PS$^{\cdot}$ + H_2O.

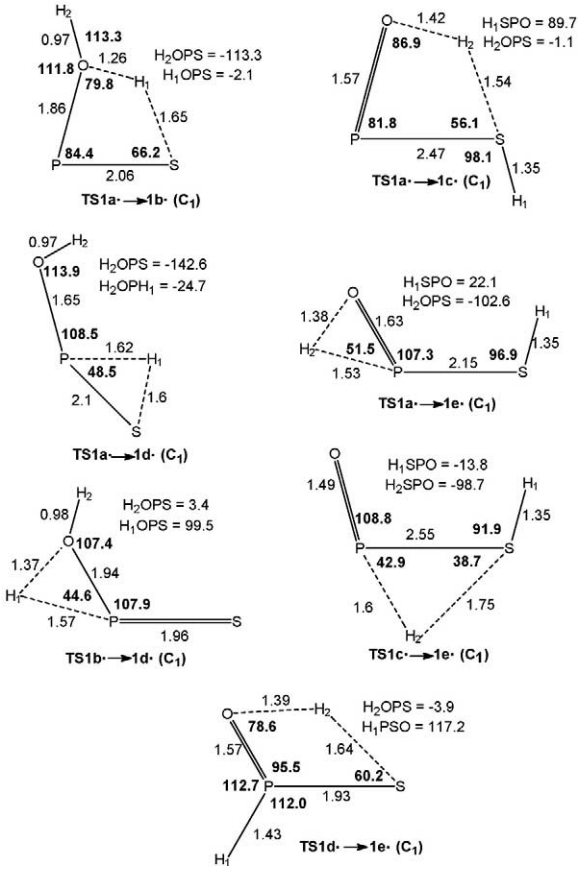

Figure 6. Selected transition-state geometries of neutral [P, S, O, H_2]$^{\cdot}$ isomers **1a**$^{\cdot}$–**1e**$^{\cdot}$ from B3LYP/6-31G(d,p) calculations.

Similarily, vertical neutralization of $\mathbf{1c}^+$ yields $\mathbf{1c}^{\cdot}$ radicals with an internal energy of 25 kJ mol^{-1} which is sufficient to induce fragmentation leading to $PO^{\cdot} + H_2S$. These neutral species can undergo further dissociation to form various fragments such as $P^{\cdot}$, S, $SH^{\cdot}$ along with H_2O and H_2S, which upon reionization can contribute to the enhancement of the signals at *m/z* 31 (P^+), *m/z* 32 ($S^{+\cdot}$), *m/z* 33 (SH^+), *m/z* 18 ($H_2O^{+\cdot}$) and *m/z* 34 ($H_2S^{+\cdot}$) in the NR spectrum. The Frank-Condon energy in vertically formed $\mathbf{1b}^{\cdot}$ and $\mathbf{1c}^{\cdot}$ may be due to the difference in geometry of $\mathbf{1b}^{\cdot}$ and $\mathbf{1c}^{\cdot}$ which are of C_S symmetry compared with $\mathbf{1b}^+$ and $\mathbf{1c}^+$ which have C_1 symmetry (Figures 2 and 5).

We have also examined the Frank-Condon factors (Table 2) for the vertical electron-transfer processes for $\mathbf{1d}^+$ and $\mathbf{1e}^+$. According to the calculated vertical recombination energies, the minimum excess Frank-Condon energy of $\mathbf{1d}^{\cdot}$ is 97 kJ mol^{-1} which is sufficient for isomerization to $\mathbf{1a}^{\cdot}$, and that of $\mathbf{1e}^{\cdot}$ is 113 kJ mol^{-1}, sufficient for isomerization to $\mathbf{1c}^{\cdot}$ which undergoes dissociation. Thus, these effects may account for the enhanced peaks in the NR spectrum as well as the moderately abundance survivor signal for $HSPOH^{\cdot}$ ($\mathbf{1a}^{\cdot}$).

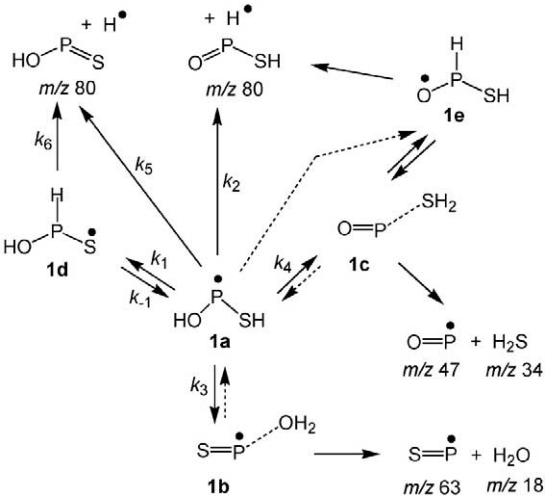

Scheme 4

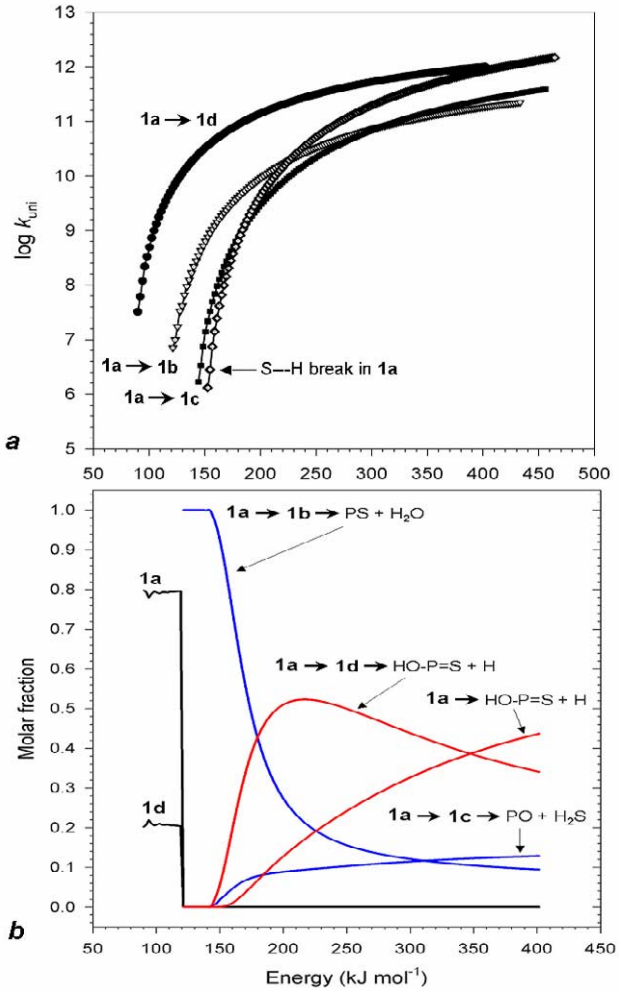

Figure 7. (**a**) RRKM rate constants (log k) calculated from the effective CCSD(T)/6-311 ++ G(3df,2p) transition-state energies. (**b**) Branching ratios for isomerizations and dissociations of $\mathbf{1a}^{\cdot}$ and $\mathbf{1d}^{\cdot}$.

The competing dissociations of $\mathbf{1a}^{\cdot}$ were analyzed by RRKM calculations of all pertinent unimolecular rate constants. The log k plots are shown for the $\mathbf{1a}^{\cdot} \rightarrow \mathbf{1b}^{\cdot}$, $\mathbf{1a}^{\cdot} \rightarrow \mathbf{1c}^{\cdot}$, and $\mathbf{1a}^{\cdot} \rightarrow \mathbf{1d}^{\cdot}$ isomerizations, and for the dissociation of the S—H bond in $\mathbf{1a}^{\cdot}$ (Figure 7a). The RRKM calculations showed that all dissociations of $\mathbf{1a}^{\cdot}$ achieve rate constants $>10^7$ s^{-1} at internal energies within 10 kJ mol^{-1} above the corresponding transition-state energy. This explains why no substantial fraction of metastable $\mathbf{1a}^{\cdot}$ was detected by variable-time NR mass spectra in the 440 ns to 4.6 μs time window. The full kinetic scheme for the dissociations and isomerizations of $\mathbf{1a}^{\cdot}$ is given in Scheme 4. The rate determining and kinetically relevant processes are shown with full arrows, the others are shown with broken arrows.

Because of the generally large unimolecular rate constants predicted by RRKM, the kt terms for dissociations on the NR time scale are large, and the kinetics can be expressed by time-independent branching ratios (Figure 7b). These show that non-dissociating $\mathbf{1a}^{\cdot}$ and $\mathbf{1d}^{\cdot}$ establish a 79:21 equilibrium in the 89–120 kJ mol^{-1} energy interval. The isomerization to $\mathbf{1b}^{\cdot}$ followed by dissociation to $PS^{\cdot}$ and H_2O dominates in the energy interval of 120–150 kJ mol^{-1}. Loss of $H^{\cdot}$ through $\mathbf{1d}^{\cdot} \rightarrow HO-P=S$ and by direct cleavage of the S—H bond in $\mathbf{1a}^{\cdot}$ dominates at high internal energies. Note that these dissociations are unresolved in the NR mass spectra without isotope labeling. The isomerization $\mathbf{1a}^{\cdot} \rightarrow \mathbf{1c}^{\cdot}$ followed by dissociation to $PO^{\cdot}$ and H_2S appears to be the least efficient one and is calculated to achieve a maximum 13% of the overall dissociation (Figure 7b).

The RRKM branching ratios are now compared with the product formation observed in the NR mass spectra. In keeping with the NR data, the calculations predict a

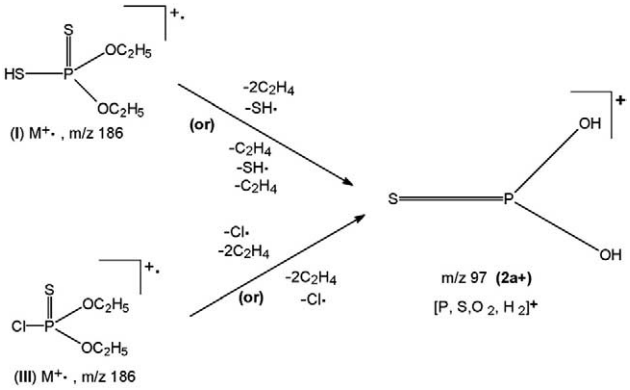

Scheme 5

fraction of non-dissociating **1a**· and another nondissociating fraction at equilibrium with **1d**·. Loss of H leading to the *m/z* 80 fragment, elimination of H_2O leading to *m/z* 63, and elimination of H_2S leading to *m/z* 47 and 34 are predicted to be kinetically competitive, in qualitative agreement with the NR data. A quantitative match of the RRKM branching ratios with the product distribution in the NR mass spectra was not attempted, because it would necessitate considering also the reionization cross sections for all neutral species, their post-reionization dissociations, and high-energy processes originating from excited electronic states. We note that PO· was reported to have an unusually high reionization cross section [20], which may contribute to the dominant *m/z* 47 peak in the NR mass spectrum.

Preparation and Dissociation of $[P,S,O_2,H_2]^+$ Ions

The 70-eV electron-ionization mass spectra of diethyl dithiophosphate (**I**), and diethyl chlorothiophosphate (**III**) yield an abundant peak at *m/z* 97 (90 and 70% of the base peak, respectively) corresponding to $[P,S,O_2,H_2]^+$ ions. The elemental composition of this ion has been confirmed by high-resolution measurements and isobaric impurities were not detected. The formation of these ions from the molecular ion of diethyl dithiophosphate ($\mathbf{I}^{+\cdot}$), can be envisaged to proceed by two different routes, (1) $186^{+\cdot}$ ($I^{+\cdot}$) → 153^+ → 125^+ → 97^+, i.e., loss of SH· radical followed by successive losses of two ethylene molecules, (2) $186^{+\cdot}$ ($\mathbf{I}^{+\cdot}$) → $158^{+\cdot}$ → 125^+ → 97^+, i.e., loss of ethylene molecule followed by successive losses of SH· radical and ethylene molecule. For $\mathbf{III}^{+\cdot}$, two different fragmentation pathways also generate the *m/z* 97 ions: (1) $188^{+\cdot}$ ($\mathbf{III}^{+\cdot}$) → 153^+ → 125^+ → 97^+, i.e., loss of Cl· radical followed by successive losses of two ethylene molecules, (2) $188^{+\cdot}$ ($\mathbf{III}^{+\cdot}$) → $160^{+\cdot}$ → $132^{+\cdot}$ → 97^+, i.e., losses of two successive ethylene molecules followed by loss of Cl· radical (Scheme **5**). Evidence for these pathways follows from metastable ion (MI) spectra of the molecular ions and the intermediate ions.

The metastable-ion spectrum of *m/z* 97 ions from $\mathbf{I}^{+\cdot}$ shows abundant SPO^+ (*m/z* 79), $P(OH)_2^+$ (*m/z* 65) ions, and low abundance OPO^+ (*m/z* 63) ions corresponding to losses of H_2O, S, and H_2S, respectively. The MI peak corresponding to loss of H_2O from $\mathbf{I}^{+\cdot}$ shows a Gaussian profile, which was characterized by the value of kinetic energy release at half-maximum, $T_{0.5}$ = 0.055 eV (55.1 meV). The kinetic energy release for loss of H_2O from *m/z* 97 ions of diethyl chlorothiophosphate (**III**) at half-maximum, $T_{0.5}$ = 0.055 eV (54.9 meV). This indicates that *m/z* 97 ions produced from both **I** and **III** have a similar structure.

The B/E and MIKES CID spectra of *m/z* 97 ions display the base peak at *m/z* 65, and the other abundant fragment ions are at *m/z* 96 (loss of H·), *m/z* 79, *m/z* 63, and *m/z* 47 ($PO^{+\cdot}$). Weakly intense peaks are observed at *m/z* 80 $[SPOH]^{+\cdot}$, *m/z* 64 $[OPOH]^+$, *m/z* 48 $[POH]^{+\cdot}$, and a cluster of peaks at *m/z* 31–33 attributable to P^+, $S^{+\cdot}$, and SH^+. All these structure indicative peaks suggests the connectivity $S = P(OH)_2^+$ ($\mathbf{2a}^+$) for the *m/z* 97 ions. The CID spectra of the *m/z* 97 ions from diethyl chlorothiophosphate (**III**) are identical with those of diethyl dithiophosphate (**I**). The representative CID spectra are presented in Figure 8a and b. The CID spectrum of the metastably generated *m/z* 97 ions from the *m/z* 125 precursor ion from **I** is found to be closely similar to the Figure 8b, suggesting that the source generated *m/z* 97 ions are largely $\mathbf{2a}^+$.

Ion Structures and Energetics

From the computational results presented in Table 4, the potential energy diagram of Scheme **6**, and the optimized ion structures shown in Figure 9, it follows that all the four isomeric ions $\mathbf{2a}^+$ to $\mathbf{2d}^+$ are minima on the potential energy surface. Ion $\mathbf{2a}^+$ is the most stable structure of the four studied. It has a C_S symmetry with an anti-anti arrangement of the two O—H bonds with respect to P = S that corresponds to the lowest-energy orientation of the corresponding bond dipoles. $\mathbf{2b}^+$ is second most stable structure, 50 kJ mol^{-1} less stable than $\mathbf{2a}^+$. Ions $\mathbf{2a}^+$ and $\mathbf{2b}^+$ are separated by an energy barrier (140 kJ mol^{-1} above $\mathbf{2b}^+$), which is below the lowest dissociation threshold. $\mathbf{2c}^+$, 105 kJ mol^{-1} less stable than $\mathbf{2a}^+$, has a 20% longer P—OH_2 bond and can preferably dissociate into SPO^+ (*m/z* 79) and H_2O which requires 180 kJ mol^{-1}. Ions $\mathbf{2a}^+$ and $\mathbf{2c}^+$ are separated by an energy barrier (85 kJ mol^{-1} above $\mathbf{2c}^+$), which is below the dissociation energy for the formation of $SPO^+ + H_2O$. Similarly, $\mathbf{2d}^+$, 147 kJ mol^{-1} less stable than $\mathbf{2a}^+$, has a longer P—SH_2 bond (12%) and can preferably dissociate into OPO^+ (*m/z* 63) and H_2S, which requires 246 kJ mol^{-1}. It should be noted that this high-energy requirement is in line with the low abundance of *m/z* 63 ions in the CID spectrum. Ions $\mathbf{2b}^+$ and $\mathbf{2d}^+$ are separated by an energy barrier (94 kJ mol^{-1} above $\mathbf{2d}^+$), which is below the dissociation energy for the formation of $OPO^+ + H_2S$. Thus, the calculated energies imply that $\mathbf{2a}^+$ can isomerize to $\mathbf{2b}^+$ and $\mathbf{2c}^+$

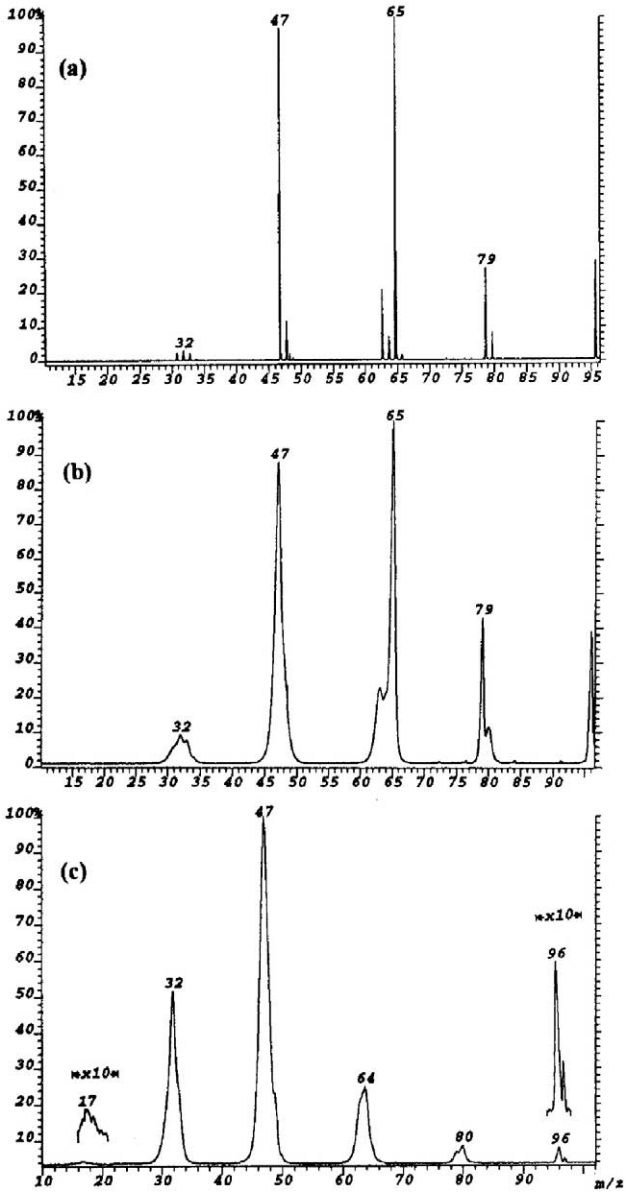

Figure 8. (**a**) B/E-CID spectrum (O_2, 70% transmission), (**b**) MIKES-CID spectrum (O_2, 70% transmission), and (**c**) NR spectrum (Xe, 70% T/O_2, 70% transmission) of *m/z* 97 ions from diethyl dithiophosphate (**I**).

before dissociation. Some of the $\mathbf{2b}^+$ ions can isomerize to $\mathbf{2d}^+$ before the dissociation into $OPO^+ + H_2S$. Thus, based on these results, it can be proposed that the *m/z* 97 ions are a mixture of $\mathbf{1a}^+/\mathbf{1b}^+/\mathbf{1c}^+/\mathbf{1d}^+$ ions. Again, for energetic and entropic reasons, most of the ions are expected to have the connectivity $\mathbf{1a}^+$. The calculated dissociation energies for various fragmentation channels are in fairly good agreement with the fragment ion abundances in the CID mass spectrum. For example, the base peak in the spectrum at *m/z* 65 [$P(OH)_2^+$] corresponds to the lowest energy fragmentation channel. The intensities of other peaks in the spectrum are also in keeping with the calculated fragmentation energies given in Table 4.

Table 4. Relative energies of [P, S, O_2, H_2]$^+$ ions

	Relative energy[a]		
Species	G2	G2(MP2)	B3LYP[bc]
S═$P(OH)_2^+$ (**2a**$^+$) (C_S)	0	0	0
O═P(SH)OH^+ (**2b**$^+$) (C_1)	35	35	50
S═P(═O)OH_2^+ (**2c**$^+$) (C_1)	120	118	105
O═P(═O)SH_2^+ (**2d**$^+$) (C_S)	150	149	147
TS **2a**$^+$ → **2b**$^+$ (C_S)	183	180	189
TS **2a**$^+$ → **2c**$^+$ (C_S)	202	200	190
TS **2b**$^+$ → **2d**$^+$ (C_1)	245	242	241
$P(OH)_2^+$ + (^{3}P)S *m/z* 65	277	282	218
SPO^+ + H_2O *m/z* 79	272	261	285
$SPOH^{+\cdot}$ + $OH^\cdot$ *m/z* 80	450	454	384
OPO^+ + H_2S *m/z* 63	405	398	392
$SP(O)OH^{+\cdot}$ + $H^\cdot$ *m/z* 96	425	427	405

[a]In units of kJ mol^{-1} at 0 K.
[b]Calculations with the 6-31G(d,p) basis set.
[c]ZPE corrected.

Preparation and Dissociation of [P,S,O_2,H_2]$^\cdot$ Radicals

The neutralization (Xe, 70%)-reionization (O_2, 70%) mass spectrum of *m/z* 97 ions shows a very weak recovery signal corresponding to the survivor ions of reionized [P,S,O_2,H_2] radicals (Figure 8c). This spectrum is different from the CID spectrum of Figure 8b with respect to the fragment ion abundances. In contrast to the CID spectrum, the NR spectrum shows low abundance peaks at *m/z* 79 and 65 and highly abundant *m/z* 47 and 32 peaks. The formation of abundant *m/z* 47 is a characteristic dissociation of oxygenated phosphorous radicals [23, 32]. The spectrum also shows a peak at *m/z* 64 which is probably due to the greater stability of the neutral O = POH (*m/z* 64) molecule as opposed the formation of $P(OH)_2$·. Low-abundance peaks at *m/z* 16–18 are also present in the spectrum. The presence of a weak recovery signal, although of very low abun-

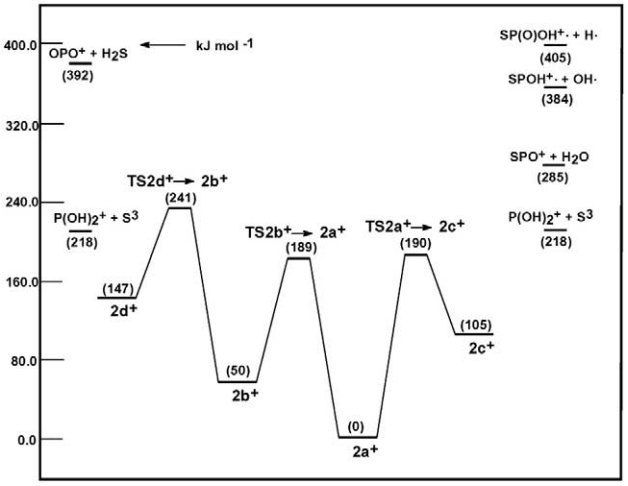

Scheme 6. Potential energy diagram from B3LYP/6-31G(d,p) calculations for the rearrangement and dissociation reactions of [P, S, O_2, H_2]$^+$ cations.

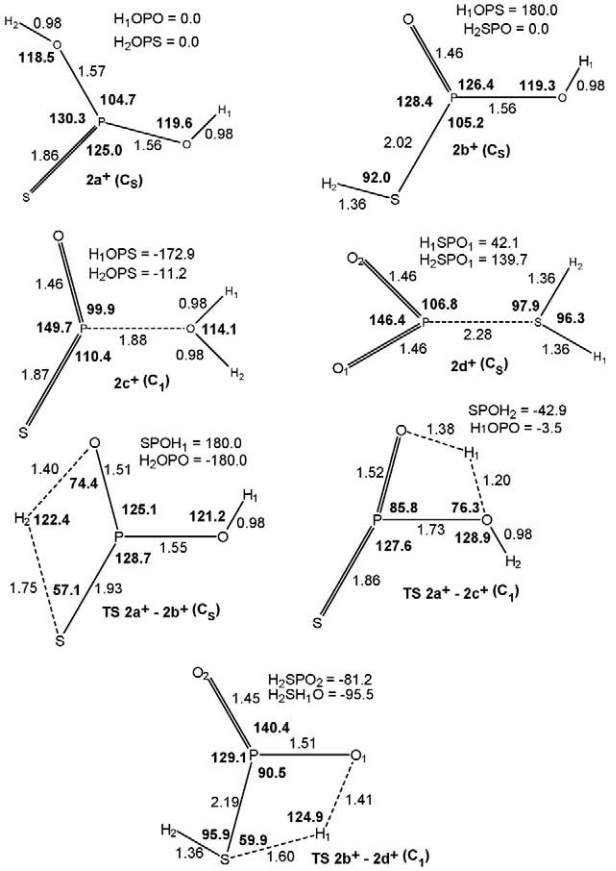

Figure 9. Selected optimized geometries of ionic [P, S, O_2, H_2]$^+$ isomers **2a**$^+$–**2d**$^+$ and connecting transition states from B3LYP/6-31G(d,p) calculations.

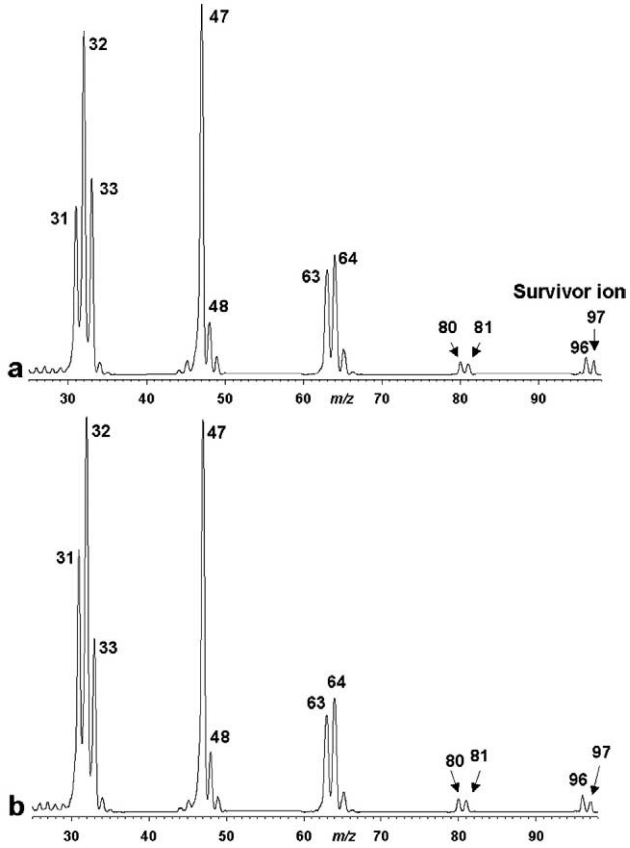

Figure 10. Neutralization (70% transmittance)/reionization O_2 (70% transmittance) mass spectra of **2a**$^+$ at (**a**) 5.0 μs and (**b**) 0.48 μs neutral dissociation times. Low-intensity peaks at *m/z* 26–29 are due to low-level isobaric hydrocarbon contaminants.

dance, indicates that vertical neutralization of **2a**$^+$ ions yield neutral species that are (kinetically) stable on the NR experimental time-scale of microseconds and have retained the **2a**$^\cdot$ connectivity.

Survivor ion is also detected in NR mass spectra obtained with dimethyl disulfide as the electron donor that were measured at 0.48 and 5.0 μs for neutral dissociation times (Figure 10a and b). These NR mass spectra are virtually time-independent, which attests to rapid dissociations of **2a**$^\cdot$ radicals at internal energies above the relevant transition states.

The difference in the abundances of the fragment ions may be due to the contribution from the dissociation of vibrationally excited [P, O_2, S, H_2] radicals, as will be discussed in the later part of the paper. According to the calculated recombination energies of ion structures **2a**$^+$–**2d**$^+$ (Table 5), electron-transfer from Xe (IE = 12.13 eV) is about 4 eV endothermic, which may cause excitation in the radicals formed.

Radical Structures and Energetics

In line with the experimental results, our theoretical calculations (Table 6 and Scheme 7) predict that **2a**$^\cdot$ is the global minimum with C_1 symmetry (Figure 11). Similar to the stability order of isomeric ions, **2b**$^\cdot$ is second most stable structure, 13 kJ mol^{-1} less stable than **2a**$^\cdot$. The **2a**$^\cdot$ and **2b**$^\cdot$ radicals are separated by an energy barrier (119 kJ mol^{-1} above **2b**$^\cdot$), which is 50 kJ mol^{-1} above the lowest dissociation threshold into OPOH + SH$^\cdot$ (Scheme 7). **2c**$^\cdot$, 71 kJ mol^{-1} less stable than **2a**$^\cdot$ has a 48% longer P—OH_2 bond than standard P—OH bond and can preferably dissociate into SPO$^\cdot$ (*m/z* 79) and H_2O which requires 29 kJ mol^{-1}. **2a**$^\cdot$ and **2c**$^\cdot$ are separated by an energy barrier (60 kJ mol^{-1} above **2c**$^\cdot$), which is 30 kJ mol^{-1} above the dissociation energy for the formation of SPO$^\cdot$ + H_2O. Similarily, **2d**$^\cdot$, 84 kJ

Table 5. Calculated adiabatic energies (IE_a) and vertical one-electron transition energies (in eV) of ions and neutrals of [P, S, O_2, H_2]$^{+\cdot}$ isomers at the B3LYP/6- 31G(d,p) level

Transitions	IE_a[A]	RE_v	IE_v
2a$^+$ → **2a**$^\cdot$	7.77	5.43	
2a$^\cdot$ → **2a**$^+$			9.11
2b$^+$ → **2b**$^\cdot$	8.15	6.16	
2b$^\cdot$ → **2b**$^+$			9.12
2c$^+$ → **2c**$^\cdot$	8.12	6.11	
2c$^\cdot$ → **2c**$^+$			9.48
2d$^+$ → **2d**$^\cdot$	8.35	6.75	
2d$^\cdot$ → **2d**$^+$			9.75

Table 6. Relative energies of [P, S, O_2, H_2]* radicals

Species	Relative energy[a] G2	G2(MP2)	B3LYP[bc]
S=P(OH)$_2^{\cdot}$ (**2a**$^{\cdot}$) (C_1)	0	0	0
O=P(SH)OH$^{\cdot}$ (**2b**$^{\cdot}$) (C_1)	10	10	13
S=P(=O)OH$_2^{\cdot}$ (**2c**$^{\cdot}$) (C_1)	78	73	71
O=P(=O)SH$_2^{\cdot}$ (**2d**$^{\cdot}$) (C_1)	—	—	84
TS **2a**$^{\cdot}$ → **2b**$^{\cdot}$ (C_1)	130	128	132
TS **2a**$^{\cdot}$ → **2c**$^{\cdot}$ (C_1)	151	149	130
TS **2b**$^{\cdot}$ → **2d**$^{\cdot}$ (C_1)	153	152	140
OPOH (*m/z* 64) + SH	89	91	82
OPO$^{\cdot}$ (*m/z* 63) + H_2S	98	96	100
SPO$^{\cdot}$ (*m/z* 79) + H_2O	91	87	100
SP(O)OH (*m/z* 96) + H$^{\cdot}$	159	156	197
SPOH (*m/z* 80) + OH$^{\cdot}$	230	229	217
P(OH)$_2^{\cdot}$ (*m/z* 65) + (^{3}P)S	314	321	279

[a]In units of kJ mol^{-1} at 0 K.
[b]Calculations with the 6-31G(d,p) basis set.
[c]ZPE corrected.

mol^{-1} less stable than **2a**$^{\cdot}$, has a longer P—SH_2 bond (39%) and can preferably dissociate into OPO$^{\cdot}$ (*m/z* 63) and H_2S which requires 15 kJ mol^{-1}. **2d**$^{\cdot}$ and **2b**$^{\cdot}$ radicals are separated by an energy barrier (56 kJ mol^{-1} above **2d**$^{\cdot}$), which is 40 kJ mol^{-1} above the dissociation energy for the formation of OPO$^{\cdot}$ + H_2S. The calculated dissociation energies of the neutrals **2a**$^{\cdot}$–**2d**$^{\cdot}$ are also in keeping with the intensities of fragment ions in the NR spectrum. The low or insignificant abundance of *m/z* 65 and 79 peaks is in keeping with the high-energy requirement of 279 kJ mol^{-1} and 100 kJ mol^{-1}, respectively, compared with the moderately abundant *m/z* 64 peak which requires only 82 kJ mol^{-1}.

To rationalize the weak recovery signal and the differences observed between the CID and NR spectra, we have examined the Franck-Condon effects on vertical electron-transfer processes in the NR experiment. For **2a**$^+$, the calculated vertical ionization energy of the

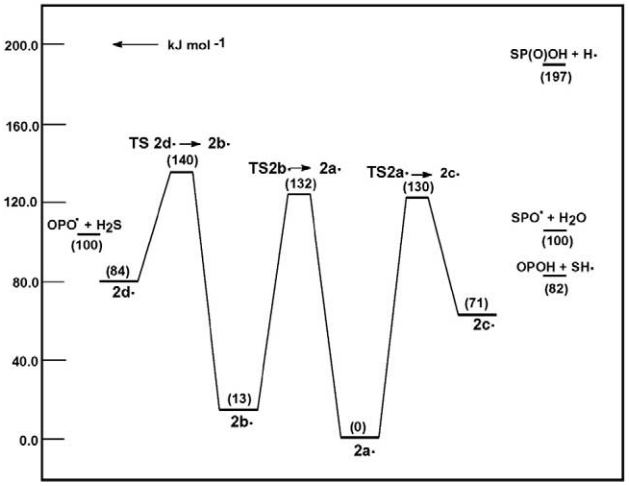

Scheme 7. Potential energy diagram from B3LYP/6-31G(d,p) calculations for the rearrangement and dissociation reactions of [P, S, O_2, H_2]$^{\cdot}$ radicals.

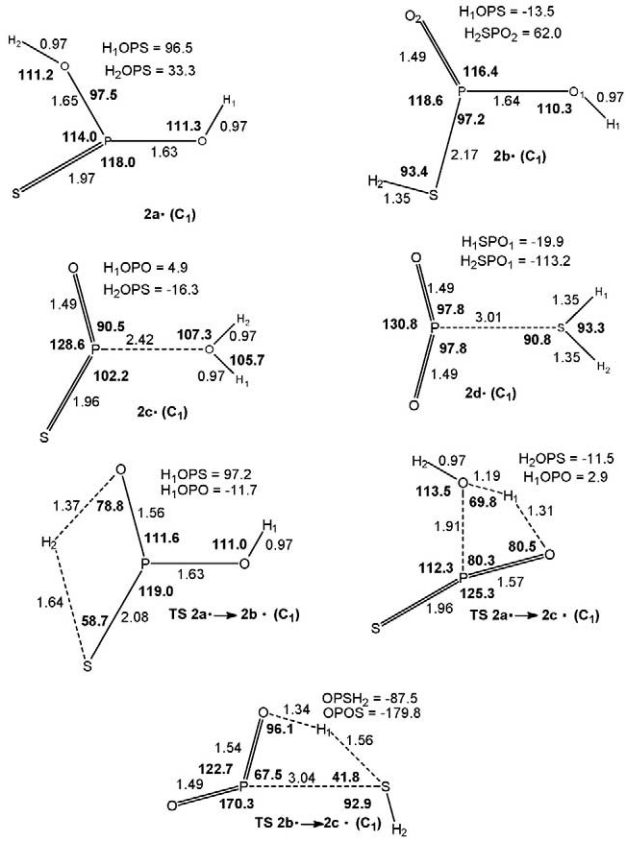

Figure 11. Selected optimized geometries of neutral [P, S, O_2, H_2]$^{\cdot}$ isomers **2a**$^{\cdot}$–**2d**$^{\cdot}$ and connecting transition states from B3LYP/6-31G(d,p) calculations.

neutral (IE_V) is found to be 129 kJ mol^{-1} (Table 5) higher than the adiabatic process, and vertical neutralization (RE_V) of thermalized **2a**$^+$ ions differ by 226 kJ mol^{-1} from the adiabatic process. Thus, the NR experiment is associated with unfavorable Franck-Condon process in both the directions leading to the formation of vibrationally excited neutral and the reionized **2a**$^+$ [47]. The excess Frank-Condon energy of **2a**$^{\cdot}$ is sufficient to induce isomerization as well as dissociation (Table 5). Likewise, vertical neutralization of **2b**$^+$–**2d**$^+$ leads to the corresponding excited radicals of **2b**$^{\cdot}$–**2d**$^{\cdot}$ and their Franck-Condon energies are 192 kJ mol^{-1}, 194 kJ mol^{-1}, and 155 kJ mol^{-1}, respectively. From Table 6 and Scheme 7, clearly these energies are sufficient for dissociation of these transient radicals. These effects are consistent with the considerable geometry differences between the **2a**$^+$–**2d**$^+$ ions and the corresponding radicals (Figure 9 and Figure 11). As a result of the deep dissociation of these transient radicals, various fragments such as PO, S, and P neutrals are formed which upon reionization contribute to the enhanced peaks at *m/z* 47, 32, and 31. Thus, the observed Franck-Condon effects provide a rationale for the observed differences between the CID and NR spectra also for the weak but discrete recovery signal corresponding to the kinetically stable survivor ions of S = $P(OH)_2$.

Conclusions

Radicals **1a**$^{\cdot}$ and **2a**$^{\cdot}$ are intrinsically stable species in an isolated state in the gas-phase. When generated from their corresponding cations by collisional electron transfer, the radicals acquire substantial internal energies by Franck-Condon effects that promote their isomerizations and dissociations. The dissociations observed in the NR mass spectra are qualitatively accounted for by RRKM calculations on ab initio potential energy surfaces, which predict several competitive processes to occur depending on the radicals internal energy.

Acknowledgments

The authors thank Dr. J. S. Yadav, Director, IICT, Hyderabad, for facilities and Dr. M. Vairamani for cooperation. RS and PNR are grateful to CSIR, New Delhi, for financial support. KBP thanks DST, New Delhi, for the funding. F T thanks the U.S. National Science Foundation for financial support (grant CHE-0349595 for experiments and grant CHE-0342956 for computations).

References

1. Cowley, A. H. Stable Compounds with Double Bonding Between the Heavier Main-Group Elements. *Acc. Chem. Res.* **1984,** *17,* 386–392.
2. Cowley, A. H. Double Bonding Between the Heavier Main-Group Elements: From Reactive Intermediates to Isolable Molecules. *Polyhedron* **1984,** *3,* 389–432.
3. Schoeller, W. W. Bonding Properties of Low Coordinated Phosphorus Compounds. In Multiple Bonds and Low Coordinationin Phosphorus Chemistry; Regitz, M.; Scherer, O., Eds.; Georg Thieme Verlag: Stuttgart, 1990; Chap. B, pp 5–32.
4. Scherer, O. J. Phosphorus, Arsenic, Antimony, and Bismuth Multiply Bonded System with Low Coordination Number: Their Role as Complex Ligands. *Angew. Chem. Int. Ed. Engl.* **1985,** *97,* 905, 924–943.
5. Sanchez, M.; Mazieres, M. R.; Lamande, L.; Wolf, R. Phosphenium Cations. In *Multiple Bonds and Low Coordination in Phosphorus Chemistry*; Regitz, M.; Scherer, O., Eds.; Georg Thieme Verlag: Stuttgart, 1990; Chap. D, pp 129–148.
6. Kruger, G. J.; Lotz, S.; Linford, L.; Vandtk, M.; Raubenheimer, H. G. Sulfur Containing Metal-Complexes. 23. Synthesis of New Complexes Containing the $Fe_2(CO)_6S_2$ Butterfly Unit. Crystal and Molecular Structure of $[Fe_2(CO)_6(\eta$- $S_2P(C_6H_4OMe$-P)$Fe(CO)_4]$, Determined from Two Different Crystal Modifications. *J. Organomet. Chem.* **1985,** *280,* 241–251.
7. Lindner, E.; Auch, K.; Weiss, G. A.; Hiller, W.; Fawzi, R. Preparation and Properties of, and Reactions with, Metal-Containing Heterocycles. 53. Stabilization of Thiophosphanes and Dithiophosphoranes with Carbonyl Metal Complexes. *Chem. Ber.* **1986,** *119,* 3076–3088.
8. Wesdemiotis, C.; McLafferty, F. W. Neutralization Reionization Mass Spectrometry (NRMS). *Chem. Rev.* **1987,** *87,* 485–500.
9. Holmes, J. L. The Neutralization of Organic Cations. *Mass Spectrom. Rev.* **1989,** *8,* 513–539.
10. Tureček, F. The Modern mass Spectrometer. A Laboratory for Unstable Neutral Species. *Org. Mass Spectrom.* **1992,** *27,* 1087–1097.
11. Zagorevski, D. V.; Holmes, J. L. Neutralization-Reionization Mass Spectrometry Applied to Organometallic and Coordination Chemistry. *Mass Spectrom. Rev.* **1994,** *13,* 133–154.
12. Goldberg, N.; Schwarz, H. Neutralization-Reionization Mass Spectrometry. A Powerful Laboratory to Generate and Probe Elusive Neutral Molecules. *Acc. Chem. Res.* **1994,** *27,* 347–352.
13. Zagorevski, D. V.; Holmes, J. L. Neutralization-Reionization Mass Spectrometry Applied to Organometallic and Coordination Chemistry (Update: 1914–1998). *Mass Spectrom. Rev.* **1999,** *18,* 87–118.
14. Tureček, F. Transient Intermediates of Chemical Reactions by Neutrailization-Reionization Mass Spectrometry. *Top. Curr. Chem.* **2003,** *225,* 77–129.
15. Keck, H.; Kuchen, W.; Renneberg, H.; Terlouw, J. K.; Visser, H. C. RS − P = S in the Gas Phase. First Generation of (Organothio)Thiophosphanes. *Angew. Chem. Int. Ed. Engl.* **1991,** *30,* 318–320.
16. Keck, H.; Kuchen, W.; Renneberg, H.; Terlouw, J. K. On the Existence of H_3PS and Its Radical Cation in the Gas Phase. *Phosphorus. Sulfur Relat. Elem.* **1988,** *40,* 227–232.
17. Keck, H.; Kuchen, W.; Renneberg, H.; Terlouw, J. K.; Visser, H. C. Gaseous H_3PS_2. Generation and Characterization. *Z. Anorg. Allg. Chem.* **1990,** *580,* 181–187.
18. Wong, T.; Terlouw, J. K.; Keck, H.; Kuchen, W.; Tommes, P. The Thioxophosphane H − P = S and Its Tautomer H-S-P, (Thiohydroxy) Phosphinidene, are Stable in the Gas Phase. *J. Am. Chem. Soc.* **1992,** *114,* 8208–8210.
19. Keck, H.; Kuchen, W.; Renneberg, H.; Schweighofer, A.; Terlouw, J. K. The Phosphorotrithious Acid $(HS)_3P$ is Stable in the Dilute Gas Phase. *Phosphorous Sulphur Silicon.* **1995,** *104,* 189–195.
20. Gu, M.; Tureček, F. The Precursor Scan. A New Type of Experiment in Neutralization-Reionization Mass Spectrometry. *Org. Mass Spectrom.* **1993,** *28,* 1135–1143.
21. Vivekananda, S.; Srinivas, R. Generation and Characterization of Ionic and Neutral (Methylthio)Oxophosphane $(CH_3SP = O)^{+\cdot/o}$ and (Methoxy)Oxophosphane $(CH_3O - P = O)^{+\cdot/o}$ by Neutralization-Reionization Mass Spectrometry. *Int. J. Mass Spectrom. Ion Processes* **1997,** *171,* 79–82.
22. Vivekananda, S.; Raghunath, P.; Bhanuprakash, K.; Srinivas, R. Characterization of Ammonia Phosphorus Oxide H_3NPO^+ Ions and Their Neutral Counterparts by Mass Spectrometry and Computational Chemistry. *Int. J. Mass Spectrom.* **2001,** *208,* 59–65.
23. Tureček, F.; Gu, M.; Hop, C. E. C. A. Franck-Condon Dominated Chemistry. Formation and Dissociations of Tetrahydroxyphosphoranyl Radicals Following Femtosecond Reduction of their Cations in the Gas Phase. *J. Phys. Chem.* **1995,** *99,* 2278–2291.
24. Gustafson, S. M.; Cramer, C. J. Ab Initio Conformational and Stereopermutational Analyses of Phosphoranyl Radicals $HP(OR)_3$ and $P(OR)_4$ [R = H or CH_3]. *J. Phys. Chem.* **1995,** *99,* 2267–2277.
25. Cramer, C. J.; Gustafson, S. M. An ab Initio Conformational and Stereopermutational Analysis of Dihydroxyphosphoranyl, $H_2P(OH)_2$. *J. Am. Chem. Soc.* **1994,** *116,* 723–734.
26. Cramer, C. J.; Gustafson, S. M. Hyperconjugation Versus Apicophilicity in Trigonal Bipyramidal Phosphorus Species. *J. Am. Chem. Soc.* **1993,** *115,* 9315–9316.
27. Cramer, C. J. Where is the Unpaired Electron in the Phosphoranyl Radicals H3PS and H3PSH? *Chem. Phys. Lett.* **1993,** *202,* 297–302.
28. Cramer, C. J. The Fluorophosphoranyl Series. Theoretical Insights into Relative Stabilities and Localization of Spin. *J. Am. Chem. Soc.* **1991,** *113,* 2439–2447.
29. Cramer, C. J. Theoretical Rotation, Pseudorotation, and Pseudoinversion Barriers for the Hydroxyphosphoranyl Radical. *J. Am. Chem. Soc.* **1990,** *112,* 7965–7972.

30. Cramer, C. J.; Dykstra, C. E.; Denmark, S. E. An Ab Initio Study of the [1, 2]. Proton Transfer from Phosphine Oxide to Phosphinic Acid. *Chem. Phys. Lett.* **1987,** *136,* 17–21.
31. Korn, M.; Oberhammer, H.; Minkwitz, R. Conformations and Structures of Thiophosphanes Containing One, Two, and Three P—S Bonds. A Gas Electron Diffraction and ab Initio Study. *J. Mol. Struct.* **1993,** *300,* 61–72.
32. Srikanth, R.; Srinivas, R.; Bhanuprakash, K.; Vivekananda, S.; Syrstad, E. A.; Tureček, F.; Generation and Characterization of Ionic and Neutral $P(OH)_2^{+/\cdot}$ in the Gas Phase by Tandem Mass Spectrometry and Computational Chemistry. *J. Am. Soc. Mass. Spectrom.* **2002,** *13,* 250–264.
33. Tureček, F.; Gu, M.; Shaffer, S. A. A Novel Tandem Quadrupole Acceleration-Deceleration Mass Spectrometer for Neutralization-Reionization Studies. *J. Am. Soc. Mass Spectrom.* **1992,** *3,* 493–501.
34. Kuhns, D. W.; Shaffer, S. A.; Tran, T. B.; Tureček, F. The Methylthiomethyl Radical. A Variable-Time Neutralization-Reionization and ab Initio Study. *J. Phys. Chem.* **1994,** *98,* 4845–4853.
35. Kuhns, D. W.; Tureček, F. Unimolecular Neutral and Ion Kinetics by Variable-Time Neutralization-Reionization Mass Spectrometry. *Org. Mass Spectrom.* **1994,** *29,* 463–469.
36. Frisch, M. J.; Trucks, G. W.; Schlegel, H. B.; Scuseria, G. E.; Robb, M. A.; Cheeseman, J. R.; Montgomergy, J. A., Jr.; Vreven, T.; Kudin, K. N.; Burant, J. C.; Millam, J. M.; Iyengar, S. S.; Tomasi, J.; Barone, V.; Mennucci, B.; Cossi, M.; Scalmani, G.; Rega, N.; Petersson, G. A.; Nakatsuji, H.; Hada, M.; Ehara, M.; Toyota, K.; Fukuda, R.; Hasegawa, J.; Ishida, M.; Nakajima, T.; Honda, Y.; Kitao, O.; Nakai, H.; Klene, M.; Li, X.; Knox, J. E.; Hratchian, H. P.; Cross, J. B.; Adamo, C.; Jaramillo, J.; Gomperts, R.; Stratmann, R. E.; Yazyev, O.; Austin, A. J.; Cammi, R.; Pomelli, C.; Ochterski, J. W.; Ayala, P. Y.; Morokuma, K.; Voth, G. A.; Salvador, P.; Dannenberg, J. J.; Zakrzewski, V. G.; Dapprich, S.; Daniels, A. D.; Strain, M. C.; Farkas, O.; Malick, D. K.; Rabuck, A. D.; Raghavachari, K.; Foresman, J. B.; Ortiz, J. V.; Cui, Q.; Baboul, A. G.; Clifford, S.; Cioslowski, J.; Stefanov, B. B.; Liu, G.; Liashenko, A.; Piskorz, P.; Komaromi, I.; Martin, R. L.; Fox, D. J.; Keith, T.; Al-Laham, M. A.; Peng, C. Y.; Nanayakkara, A.; Challacombe, M.; Gill, P. M. W.; Johnson, B.; Chen, W.; Wong, M. W.; Gonzalez, C.; Pople, J. A. *Gaussian 03, Revision B. 05*; Gaussian, Inc.: Pittsburgh, PA, 2003.
37. Becke, A. D. Density-Functional Thermochemistry. 3. The Role of Exact Exchange. *J. Chem. Phys.* **1993,** *98,* 5648–5652.
38. Curtiss, L. A.; Raghavachari, K.; Trucks, G. W.; Pople, J. A. Gaussian-2 Theory for Molecular Energies of First-Row and Second-Row Compounds. *J. Chem. Phys.* **1991,** *94,* 7221–7230.
39. Curtiss, L. A.; Raghavachari, K.; Trucks, G. W.; Pople, J. A. Gaussian-2 Theory for Molecular Energies of First-Row and Second-Row Compounds. *J. Chem. Phys.* **1993,** *98,* 1293.
40. Møller, C.; Plesset, M. S. Note on an Approximation Treatment for Many-Electron Systems. *Phys. Rev.* **1934,** *46,* 618–622.
41. Schlegel, H. B. Potential Energy Curves Using Unrestricted Moeller-Plesset Perturbation Theory with Spin Annihilation. *J. Chem. Phys.* **1986,** *84,* 4530–4534.
42. Cízek, J.; Paldus, J.; Sroubkova, L. Cluster Expansion Analysis for Delocalized Systems. *Int. J. Quantum Chem.* **1969,** *3,* 149–167.
43. Purvis, G. D.; Bartlett, R. J. A Full Coupled-Cluster Singles and Doubles Model: The Inclusion of Disconnected Triples. *J. Chem. Phys.* **1982,** *76,* 1910–1918.
44. Gilbert, R. G.; Smith, S. C. Theory of Unimolecular and Recombination Reactions; Blackwell: Oxford, UK, 1990; pp 52–135
45. Zhu, L.; Hase, W. L. *Quantum Chemistry Program Exchange*; Indiana University: Bloomington, IN, 1994; Program no. QCPE 644.
46. Frank, A. J.; Sadílek, M.; Ferrier, J. G.; Tureček, F. Sulfur Oxyacids and Radicals in the Gas Phase. A Variable-Time Neutralization-Photoexcitation-Reionization Mass Spectrometric and ab Initio/RRKM Study. *J. Am. Chem. Soc.* **1997,** *119,* 12343–12353.
47. Nguyen, V. Q.; Tureček, F. Energy Effects in Collisional Neutralization with Organic Molecules. *J. Mass Spectrom.* **1996,** *31,* 843–854.